Inversion potential for the $\alpha + {}^{12}C$ system

R. Lichtenthäler F., A. C. C. Villari, A. Lépine-Szily, and L. C. Gomes
Departamento de Física Nuclear, Instituto de Física da Universidade de São Paulo, Caixa Postal 20516, 01498 São Paulo, São Paulo, Brazil
(Received 15 March 1991)

The $\alpha + {}^{12}C$ elastic-scattering angular distributions at $E_{lab} = 120$, 145, and 172.5 MeV were phase-shift analyzed and an inversion procedure for the determination of the optical potential was applied. The potential and its associated uncertainties, as a function of the radial distance, were found. Comparison is made with usual Wood-Saxon optical potential analysis.

I. INTRODUCTION

The problem of determining the potential from the S-matrix elements at fixed energy is extensively discussed in the literature [1], and some approximate methods have been developed and applied to nuclear physics problems. For example, Lipperheide and Fiedeldey [2] based their method on the assumption that if S_l is a simple rational function of l, a simple method can be applied for the determination of $V(r)$. Another approach is the semiclassical extension of Kujawski [3] to complex potentials. A further different approach is proposed by Ioannides and Mackintosh [4] and Cooper and Mackintosh [5] based on an iterative-perturbative procedure.

For the purpose of investigating the uncertainties in the optical potential resulting from the errors associated with the experimental measurements of elastic cross sections, we found the method of Ref. [4] most convenient. Thus we adopt their procedure and employ the measurements of Wiktor *et al.* [6] for the $\alpha + {}^{12}C$ system at $E_{lab} = 120$, 145, and 172.5 MeV as our input data. Our choice of this set of data, apart from its good quality, was based on the fact that at the energies measured we expect the $\alpha + {}^{12}C$ system to be reasonably transparent, allowing a sufficiently precise determination of the optical potential. In Sec. II we describe and illustrate the inversion procedure. Section III contains a description of our analysis, and in Sec. IV we draw our major conclusions.

II. INVERSION PROCEDURE

We assume that the elastic-scattering matrix S_l is reproduced by the spherically symmetric optical potential $V(r)$ for two colliding spinless nuclei. If $V^0(r)$ is an approximation to $V(r)$ and S_l^0 its corresponding scattering matrix, the following relation is easily obtained.

$$S_l - S_l^0 = -\frac{4\mu i}{\hbar^2 k}\int_0^\infty \chi_l(r)\chi_l^0(r)[V(r)-V^0(r)]dr \ , \tag{2.1}$$

where μ is the reduced mass of the system and k the wave number for the elastic channel. $\chi_l(r)$ and $\chi_l^0(r)$ are the radial wave-function amplitudes for the angular momentum hl corresponding to $V(r)$ and $V^0(r)$, respectively. We have imposed the following normalization at infinity:

$$\chi_l(r) = \frac{i}{2}[G_l - iF_l - S_l(G_l + iF_l)] \ ,$$

at $r \to \infty$, and similarly for $\chi_l^0(r)$. F_l and G_l are the regular and irregular Coulomb wave functions as defined by Abramowitz and Stegun [7]. Equation (2.1) is the starting point for the inversion procedure.

By setting

$$\chi_l(r) = \chi_l^0(r) \ ,$$

Eq. (2.1) is transformed into a linear integral equation for the dimensionless function:

$$f(r) = [V(r) - V^0(r)]/E_0 \ ,$$

where E_0 is the kinetic energy of the ions in the elastic channel.

We assume that the nuclear potential contributes to S_l only for $l < l_{max}$. Next, we choose a basis of N linearly independent functions $y_i(r)$ to represent $f(r)$ in the interval $(0, r_{max})$. For r_{max} we may take the classical closest-approach radius for the ions in the presence of the Coulomb field with angular momentum $\hbar l_{max}$. For the $y_i(r)$ we used the linear splines, which we found to be most convenient.

With these arrangements Eq. (2.1) transforms into a set of algebraic linear equations:

$$S_l - S_l^0 \equiv \delta S_l = \sum_{i=1}^{N} B_{li} a_i, \quad 0 \le l \le l_{max} \ , \tag{2.2}$$

with

$$f(r) = \sum_{i=1}^{N} a_i y_i(r) \tag{2.3}$$

and

$$B_{li} = -2ik\int_0^\infty [\chi_l^0(r)]^2 y_i(r) dr \ . \tag{2.4}$$

The coefficients a_i are determined by taking $N < l_{max} + 1$ and minimizing the expression

$$\chi^2 = \frac{1}{l_{max} + 1 - N}\sum_{l=0}^{l_{max}} \left| \delta S_l - \sum_{i=1}^{N} B_{li} a_i \right|^2 W_l \ , \tag{2.5}$$

where W_l are weighting factors. We have taken

$$W_l=(2l+1)/(l_{\max}+1)\ .$$

The procedure can now be summarized: (i) We choose $V^0(r)$ as a starting potential; (ii) we fix $l_{\max}$, $r_{\max}$, and the linear spline basis that cover the interval $(0,r_{\max})$; (iii) we determine a_i by requiring χ^2 to be minimum; (iv) we find a new potential $V^0(r)+E_0 f(r)$; and (v) we repeat the above procedure starting with the new potential until convergence is reached.

Figure 1 exhibits an example that illustrates the procedure. The target S_l are those generated by the Wood-Saxon optical potential of Ref. [6]:

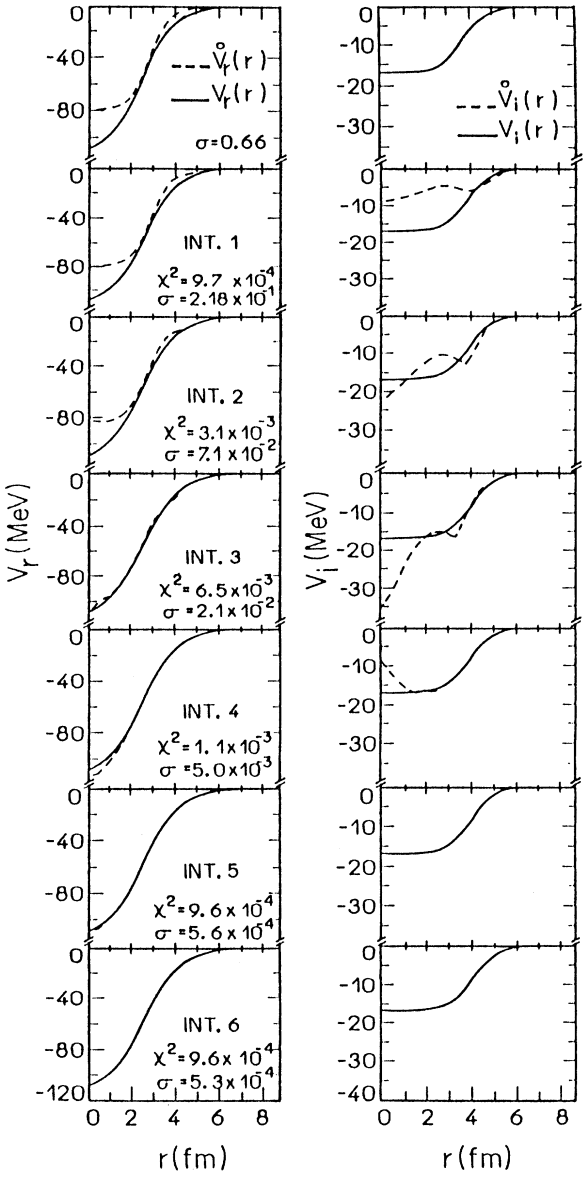

FIG. 1. Real and imaginary parts of the inversion potential after each iteration (dashed line) and the target potential of Ref. [6] (solid line).

$$V(r)=\frac{V_0}{1+\exp[(r-R)/a]}+i\frac{W_0}{1+\exp[(r-R)/a]_i},$$

$$R=r_0(A_P^{1/3}+A_T^{1/3})\ ,$$

where the parameters are given in the second column of Table I.

For the starting potential we also used a Wood-Saxon shape for the real part with parameters given in the third column of Table I with the imaginary part set to zero. We chose $l_{\max}=40$ and $r_{\max}=10$ fm and used a basis of 20 linear splines equally spaced over the interval (0,10 fm). The procedure converged after seven iterations with final $\chi^2=0.000\,96$. After each iteration we calculate the distance between the target S_l and the calculated S_l^0 matrices defined as follows.

$$\sigma=\frac{1}{l_{\max}}\sum_{o}^{l_{\max}}|S_l-S_l^0|\ .$$

Figure 1 exhibits the calculated potentials for each iteration and the respective values of χ^2 and σ. It is interesting to observe that although we started with a potential quite different from the one which originated the input S matrix, after seven interactions the procedure returns back to the same original potential. This suggests that the linearization of Eq. (2.1) does not restrict in a substantial way the applications of the procedure.

III. DATA ANALYSIS

As data, we used the measurements of elastic-scattering cross sections for the $\alpha+^{12}C$ collision at $E_{\rm lab}=120$, 145, and 172.5 MeV of Wiktor *et al.* in the angular interval from $\theta_{\rm c.m.}=6°$ to 80°, 70°, and 60°, respectively, in investigating the actual shapes and uncertainties in the optical potential determination from the experimental data. Figure 2 shows their data as dots. The solid curve is one of our optical potential fits obtained by the inversion procedure previously described. More detail will be given later. The inset in this figure is the classical deflection function obtained from the phase shifts of the 145-MeV optical potential of Ref. [6]. One should note that the experimental data cover five orders of magnitude in the cross section with errors around 5% and extend beyond the classical rainbow angle

TABLE I. First column gives the parameters, the second column their values as used in Ref. [5] for $E_\alpha=172.5$ MeV, and the third column the values of the parameters for the initial potential in the iterative procedure.

Parameters	Potential of Ref. [6]	Initial potential
V_0	112.8 MeV	80 MeV
r_0	0.673 fm	0.773 fm
a	0.82 fm	0.50 fm
W_0	16.8 MeV	0.0
r_0^i	1.076 fm	0.0
r_0^i	1.076 fm	
a_i	0.53 fm	

($\theta_{c.m.} \approx 50°$).

Since our task is to exhibit not only the shape of the potential, but also its uncertainties as determined by the data, we generated from the original data 15 new angular distributions by adding to them white noises with widths given by the experimental errors. A totality of 45 angular distributions, 15 for each energy value, was the starting point of our analysis. As the experimental angular distributions contains around 40–50 points, insufficient to make a phase-shift analysis, we enlarged the initial data set by including 50 new points for each angular distribution, determined from a cubic spline interpolation. These enlarged sets were used to search for the phase shifts that best fit the data. In the search we varied only those S_l for $0 \le l \le 25$. The other S_l values were taken from the optical potential of Ref. [6]. Figure 3 summarizes the S_l values found in our analysis. The vertical scale is $|S_l|$ and the horizontal scale is the value of l. The result is plotted as vertical bars centered on the mean value of $|S_l|$ with widths equal to twice the rms deviation from the mean value. We observe that the uncertainty in $|S_l|$ increases as l decreases, reflecting the relatively low sensitivity of the cross section to the low values of the angular momentum.

To each one of the 45 sets of S matrices, we applied the inversion procedure described in the previous section, using $l_{max}=40$, $r_{max}=10$ fm, and a base of $N=20$ linear splines. In all cases $V^0(r)$ was taken as the Wood-Saxon potential given in the third column of Table I. Figure 4 exhibits our results. The 15 optical potentials found by the inversion procedure are plotted as small dots. The open circles (connected by the dashed line) correspond to the mean value of the potentials for each radial distance. The solid curve represents the Wood-Saxon optical potential of Ref. [6]. For each energy we observe that for $r \ge 3$ fm, i.e., the surface region, the uncertainties in the potential are small and our results agree with the optical potential of Ref. [6] except for the 145-MeV case where the shape exhibits some structure outside the uncertainty bars. In the inner region df ($r < 3$ fm), the potentials deviate substantially from that of Ref. [6]. In particular, not only does the imaginary potential exhibit very large negative values, but also the real potential also becomes

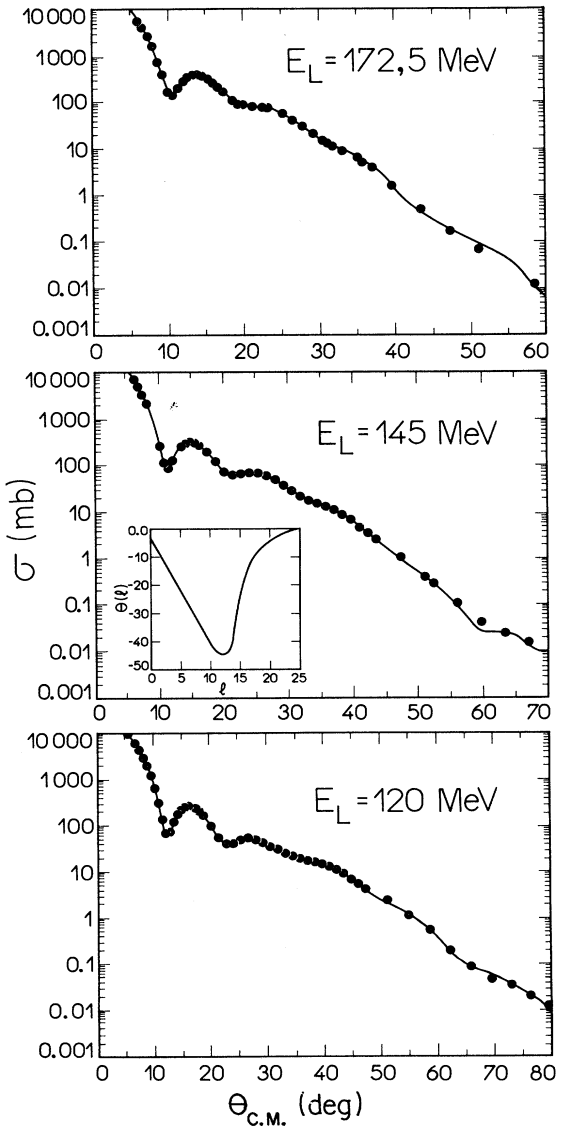

FIG. 2. Experimental elastic angular distributions of $\alpha + {}^{12}C$ at $E_\alpha = 172.5$, 145, and 120 MeV. The solid curve is one of our optical potential fits obtained by the inversion procedure. Inset: The classical deflection function obtained from the 145-MeV optical potential of Ref. [6].

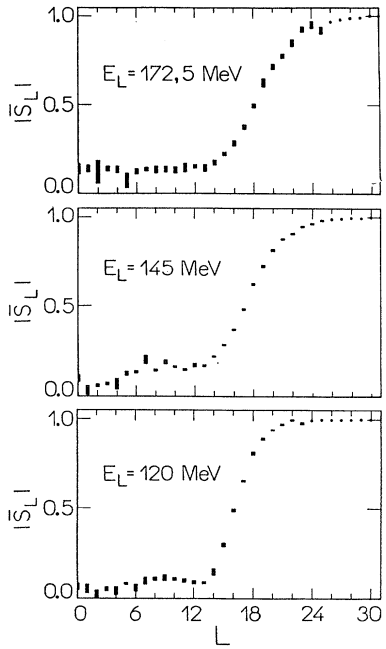

FIG. 3. Solid bars represent the rms deviation of $|S_l|$ obtained from the phase-shift analyses centered on the mean valve $|\bar{S}_l|$.

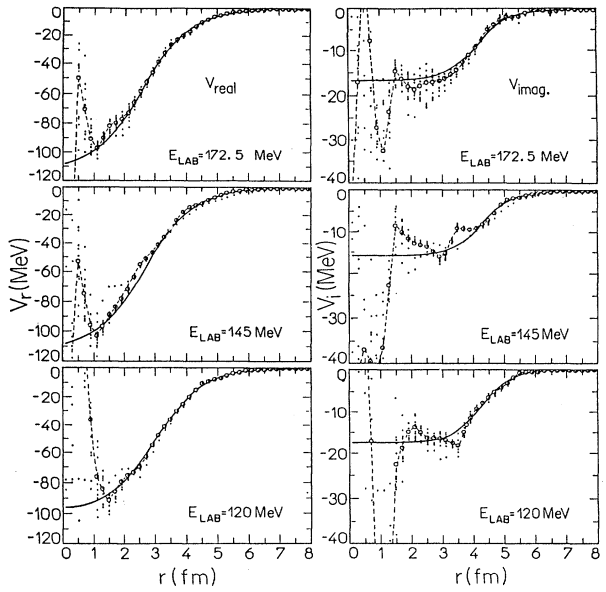

FIG. 4. Optical potentials obtained by inversion (small dots). The open circles connected by the dashed line correspond to the mean value of the potentials. The solid curves are the Wood-Saxon optical potentials of Ref. [6] for each energy.

repulsive the lower the entrance channel energy. From our point of view, these effects in the inner region as a function of the energy can be qualitatively understood as resulting from the exclusion principle that inhibits the existence of $\alpha+^{12}C$ configuration in the ^{16}O system for lower values of the excitation energy. This is in agreement with general considerations that predict the exclusion principle to be active only for $l<6$. From Fig. 4 for $E_{\rm lab}=120$ MeV, we observe that the repulsion occurs for $N<r_0=1.5$ fm, showing that the main contribution is for $l<r_0k_0=5.4$, where k_0 is the wave number for the energy under consideration. We should also point out the fact that the uncertainties in the potential get larger as the $\alpha+^{12}C$ approach one another. This basically reflects the uncertainties found in the determination of the S matrix due to the centrifugal barrier since S_l is more sensitive to the inner region for lower values of l.

IV. CONCLUSIONS

The application of the inversion procedure for the determination of the optical potential from the elastic S-matrix elements, first proposed by Ioannides and Mackintosh [4], worked well for 172.5 MeV [6]. We found both the optical potentials for the entrance channel energies measured and their uncertainties associated with the experimental errors. The uncertainties found agree with the general belief that the optical potential for ion collisions is not well determined in the inner region. Besides these main results, we also found that as the energy decreases, the imaginary part of the potential increases negatively and the real part becomes repulsive, suggesting the existence of a hard core in the inner region for low entrance channel energies. We believe that this behavior is of a general character, reflecting the constraint imposed by the exclusion principle. If this is so, then we may expect that this effect is stronger for heavier-ion collisions at the same entrance channel energy per nucleon.

We would like to thank S. Wiktor for kindly providing us with the scattering cross sections for the $\alpha+^{12}C$ system.

[1] U. Buck, Rev. Mod. Phys. **46**, 369 (1974).
[2] R. Lipperheide and H. Fiedeldey, Z. Phys. A **286**, 45 (1978).
[3] E. Kujawski, Phys. Rev. C **6**, 709 (1972).
[4] A. A. Ioannides and R. S. Mackintosh, Nucl. Phys. **A438**, 354 (1985).
[5] S. G. Cooper and R. S. Mackintosh, *Inverse Problems* **5**(5), 707 (1989).
[6] S. Wiktor, C. Mayer-Böricke, A. Kiss, M. Ragge, P. Turek, and H. Dabrowski, Acta Phys. Pol. **12**, 491 (1981).
[7] *Handbook of Mathematical Functions,* edited by M. Abramowitz and I. A. Stegun (Dover, New York, 1968).